



**AALBORG UNIVERSITY**  
DENMARK

**Aalborg Universitet**

## **Instantaneous thermal modeling of the DC-link capacitor in PhotoVoltaic systems**

Yang, Yongheng; Ma, Ke; Wang, Huai; Blaabjerg, Frede

*Published in:*

Proceedings of the 2015 IEEE Applied Power Electronics Conference and Exposition (APEC)

*DOI (link to publication from Publisher):*

[10.1109/APEC.2015.7104737](https://doi.org/10.1109/APEC.2015.7104737)

*Publication date:*

2015

*Document Version*

Early version, also known as pre-print

[Link to publication from Aalborg University](#)

*Citation for published version (APA):*

Yang, Y., Ma, K., Wang, H., & Blaabjerg, F. (2015). Instantaneous thermal modeling of the DC-link capacitor in PhotoVoltaic systems. In *Proceedings of the 2015 IEEE Applied Power Electronics Conference and Exposition (APEC)* (pp. 2733-2739). IEEE Press. I E E E Applied Power Electronics Conference and Exposition. Conference Proceedings <https://doi.org/10.1109/APEC.2015.7104737>

### **General rights**

Copyright and moral rights for the publications made accessible in the public portal are retained by the authors and/or other copyright owners and it is a condition of accessing publications that users recognise and abide by the legal requirements associated with these rights.

- Users may download and print one copy of any publication from the public portal for the purpose of private study or research.
- You may not further distribute the material or use it for any profit-making activity or commercial gain
- You may freely distribute the URL identifying the publication in the public portal -

### **Take down policy**

If you believe that this document breaches copyright please contact us at [vbn@aub.aau.dk](mailto:vbn@aub.aau.dk) providing details, and we will remove access to the work immediately and investigate your claim.

# Instantaneous Thermal Modeling of the DC-Link Capacitor in Photovoltaic Systems

Yongheng Yang, Ke Ma, Huai Wang, and Frede Blaabjerg

Department of Energy Technology  
Aalborg University  
Aalborg DK-9220, Denmark

yoy@et.aau.dk; kema@et.aau.dk; hwa@et.aau.dk; fbl@et.aau.dk

**Abstract**—Capacitors have been witnessed as one of the weak points in grid-connected PhotoVoltaic (PV) applications, and thus efforts have been devoted to the design of reliable DC-link capacitors in PV applications. Since the hot-spot temperature of the capacitor is one of the failure inducers, instantaneous thermal modeling approaches considering mission profiles for the DC-link capacitor in single-phase PV systems are explored in this paper. These thermal modelling approaches are based on: a) fast Fourier transform, b) look-up tables, and c) ripple current reconstruction. Moreover, the thermal modelling approaches for the DC-link capacitors take into account the instantaneous thermal characteristics, which are more challenging to the capacitor reliability during operation. Such instantaneous thermal modeling approaches enable a translation of instantaneous capacitor power losses to capacitor thermal loading from the operating conditions. As a consequence, it offers new insights into the temperature monitoring and reliability-oriented design of the DC-link capacitors, and thus a more reliable operation of single-phase grid-connected PV systems can be enhanced. Study results on a 3-kW single-phase grid-connected PV system have been adopted to demonstrate a look-up table based modelling approach, where real-field daily ambient conditions are considered.

## I. INTRODUCTION

In addition to the power electronics devices, the DC-link capacitors have been demonstrated to be one of the most life-limiting components in power electronics applications, like adjustable speed drives, electric vehicles, un-interruptible power supply, wind turbine systems, and grid-connected PhotoVoltaic (PV) systems [1]–[4], as it is shown in Fig. 1. As an enabling technology, the power electronics technology will be further expanded into grid-connected renewable energy systems with an increase of interest in the efficiency and the reliability [5]–[9]. Consequently, more stringent requirements (e.g., small size and longer operating time) on the DC-link capacitor are being put forward. In general, the DC-link capacitors in power electronics applications are treated as storage elements. They are responsible for balancing the DC input power from e.g., PV panels (or the DC-DC converter) and the AC output power to the grid, as it is illustrated in Fig. 1. The DC-link capacitor has also to absorb the high switching frequency ripple currents of the Pulse-Width Modulation (PWM) converters. These fundamental functions result in the basic design considerations for the DC-link capacitors – the voltage stress across the capacitor and the ripple currents/voltages.

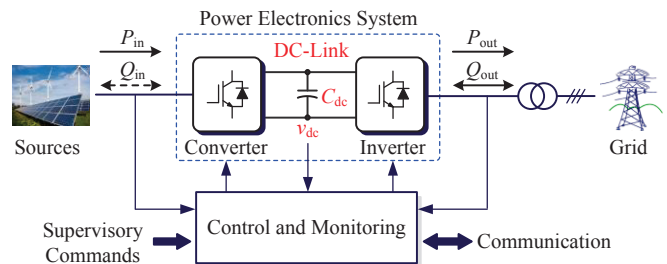


Fig. 1. Power electronics enabled grid-connected renewable energy conversion systems with a DC-link capacitor,  $C_{dc}$ .

The criteria have been widely used for the design of DC-link capacitor in the grid-connected PWM converters [3], [10]. Unfortunately, the DC-link capacitor even with an appropriate design margin based on the criteria may also fail to operate, due to the complicated operating and environmental conditions (e.g., transients like voltage sags [11] and hot areas). As a result, a failure of the entire power electronics system occurs. Hence, the reliability of the DC-link capacitors now plays an essential role in the system performance, leading to increasing efforts that are being devoted to reliability improvement and also optimization of the DC-link capacitors [3], [11]–[17]. It has been revealed that a reduction of DC-link capacitance can contribute to the use of high-reliability capacitors, e.g. film capacitors, and thus improved overall system reliability [3], [16]. In most of the prior-art studies, focuses have been put on the monitoring of the capacitor Equivalent Series Resistor (ESR) to identify whether the capacitor has been worn out (failed) or not. Thus, an in-time replacement of the DC-link capacitor can extend the reliability of the entire system. For example, in [12], a real time method to estimate the capacitor condition by diagnosing the ESR of the capacitors is introduced, and in [14], an online ESR detection method based on the capacitor’s AC losses is proposed.

Those monitoring methods can relatively indicate the health status of the capacitor, but there is still a gap between the ESR monitoring and the lifetime prediction of the capacitor, as most of the capacitor lifetime models require the hot-spot temperature information (and thus capacitor thermal models) [3], [11]. Currently, the lifetime prediction of the DC-link

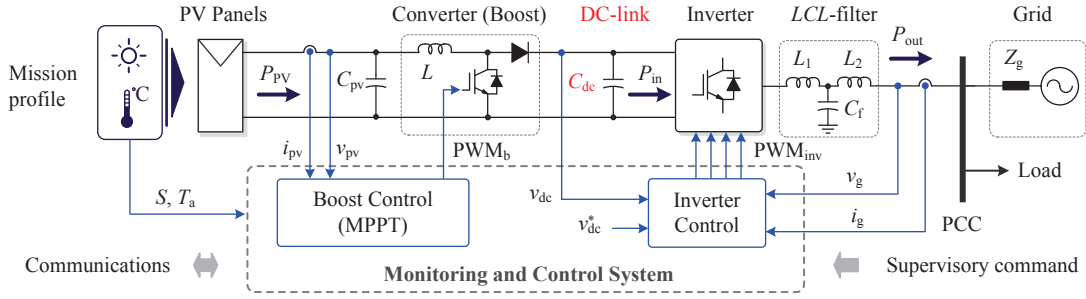


Fig. 2. Hardware schematics and overall control diagrams of a typical single-phase two-stage grid-connected PV system with an  $LCL$  filter (MPPT - Maximum power point tracking, PCC - Point of common coupling), where  $S$  is the solar irradiance,  $T_a$  is the ambient temperature, and  $Z_g$  is the grid impedance.

capacitor is based on the calculation of the power losses on the ESR, and thus it can reflect the long-term thermal performance. For instance, in [18], the mission profiles (i.e., solar irradiance and ambient temperature) have been translated into the capacitor stresses, including both electrical and thermal stresses. However, on-line predicting the lifetime of the capacitor (catastrophic failures) are more challenging, which calls for an instantaneous thermal modelling for monitoring and thus protection of the DC-link capacitors.

Hence, as an extended study of [18], this paper serves to explore the instantaneous modelling approaches for the DC-link capacitor in grid-connected single-phase PV systems. Firstly, the traditional thermal model of the DC-link capacitor is presented in § II, followed by a discussion on the frequency dependency of the capacitor equivalent series resistance. Then, focuses have been put on the instantaneous modelling approaches in § III, which can enable to monitor the instantaneous hot-spot temperature of the DC-link capacitor by measuring the capacitor currents (both low frequency and high frequency ripples). Study case on a 3-kW single-phase two-stage PV system by simulations has been provided in § IV before the conclusion of this paper.

## II. MODELING OF DC-LINK CAPACITORS

Fig. 2 shows a typical double-stage single-phase grid-connected PWM inverter system with an  $LCL$  filter. In respect to the control of this grid-connected system, it consists of two parts - the boost control aiming at Maximum Power Point Tracking (MPPT) and the inverter control targeting at a proper power injection. Normally, depending on the power ratings, the DC-link voltage  $v_{dc}$  is controlled by the inverter as a constant, e.g.,  $v_{dc}^* = 400$  V. In addition, the injected current by the PV inverter is required to be synchronized with the grid voltage, e.g., by means of a phase locked loop, and also the single-phase system should operate at unity power factor as required. Table I shows the system specifications.

Since the single-phase inverter under study has an AC power of the double-line frequency (e.g., 100 Hz), the DC-link capacitor  $C_{dc}$  has to store or release power in order to balance the power difference. Thus, there will inevitably be a double-line frequency ripple at the DC-link capacitor [3], [10], [18]. The ripple voltage amplitude  $\Delta v$  is mainly determined

TABLE I  
PARAMETERS OF THE SINGLE-PHASE TWO-STAGE GRID-CONNECTED PV SYSTEMS SHOWN IN FIG. 2.

Parameter	Value
Power rating*	$P_n = 3$ kW
Boost converter inductor	$L = 1$ mH
PV side capacitor	$C_{pv} = 220$ $\mu$ F
$LCL$ -filter	$L_1 = 2$ mH
	$L_2 = 3$ mH
	$C_f = 4.7$ $\mu$ F
Damping resistor of $LCL$ -filter	$R_d = 10$ $\Omega$
Switching frequencies	$f_b = f_{inv} = 10$ kHz
Sampling frequency	$f_s = 10$ kHz
MPPT sampling frequency	$f_{mpp} = 400$ Hz
Grid voltage amplitude	$V_{gm} = 230 \times \sqrt{2}$ V
Grid frequency	$\omega_0 = 2\pi \times 50$ rad/s

\*Installed PV capacity at 1000 W/m<sup>2</sup>, 25 °C

by the input DC power (e.g., the boost converter output) and the DC-link voltage. Ignoring the power losses on the inverter and the  $LCL$  filter, the peak to peak voltage ripple can be approximated as,

$$\Delta v \approx \frac{P_{in}}{2\pi f_g C_{dc} v_{dc}} \quad (1)$$

where  $P_{in} \approx P_{out}$  with  $P_{in}$ ,  $P_{out}$  being the inverter input power and the output power to the grid, respectively,  $f_g$  is the nominal grid frequency,  $C_{dc}$  is the capacitance of the DC-link capacitor, and  $v_{dc}$  is the DC-link voltage. Moreover, the double-line frequency ripple current of the DC-link capacitor in Root-Mean-Square (RMS) can be given as,

$$i_{c, \text{RMS}} \approx \frac{P_{in}}{\sqrt{2} v_{dc}} \quad (2)$$

Subsequently, the power losses  $P_{c, \text{loss}}$  on the DC-link capacitor can be obtained as,

$$P_{c, \text{loss}} \approx i_{c, \text{RMS}}^2 R_{\text{ESR}} \quad (3)$$

in which the  $R_{\text{ESR}}$  is the ESR of the DC-link capacitor  $C_{dc}$ , and only the double-line frequency ripple currents are taken into consideration. In addition, Eq. (1) also enables a basic component selection of the DC-link capacitance. For instance,

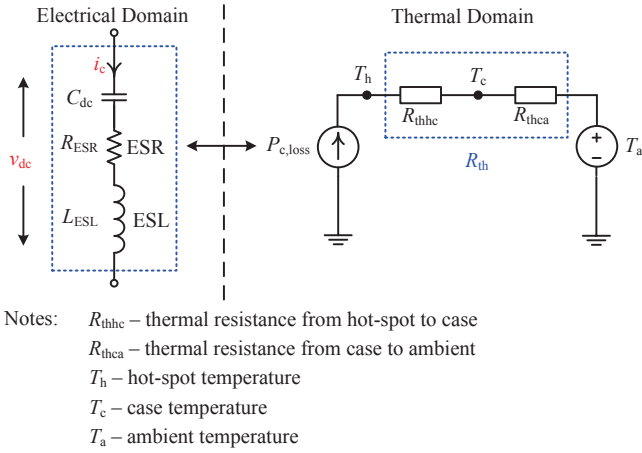


Fig. 3. Simplified thermal model of an aluminum electrolytic DC-link capacitor (from the electrical domain to thermal domain linked by power losses [19]), where the thermal capacitances are ignored.

in this study, the DC-link voltage is controlled as  $v_{dc}^* = 400 \pm 10$  V, resulting in a 5% peak to peak voltage ripple across the DC-link capacitor (i.e.,  $\Delta v = 20$  V), and thus the required DC-link capacitance is calculated as  $C_{dc} = 1200 \mu\text{F}$  according to Eq. (1) and Table I. Consequently, two capacitors of  $2200 \mu\text{F}/385$  V can be connected in series as the DC-link, which roughly can fulfill the voltage ripple and voltage stress requirements of the DC-link capacitor.

Moreover, according to Eq. (2), a higher power injection will result in a higher ripple current in the case of a constant-controlled DC-link voltage. Thus, due to the internal resistance (i.e., mainly the ESR,  $R_{ESR}$ ) of the capacitor, there will be more power losses dissipating on the DC-link capacitor, which thus contributes to a hot-spot temperature rise. This heating-up may shorten the capacitor servicing time, and also may induce a degradation of the capacitor performance, especially during transients. Consequently, monitoring the hot-spot temperature of the DC-link capacitor is becoming of more importance in order to ensure a stable operation of the PV system.

The relationship between the capacitor power losses and its hot-spot temperature can be modelled as shown in Fig. 3, which is a simplified representation of the traditional thermal model of DC-link capacitors provided by the manufacturers. In accordance to Eq. (3) and Fig. 3, the steady-state hot-spot temperature of the DC-link capacitor  $T_h$  can then be given as,

$$T_h \approx P_{c, \text{loss}} R_{th} + T_a \quad (4)$$

where  $T_h$  is the hot-spot temperature,  $T_a$  is the ambient temperature, and  $R_{th}$  is the total thermal impedance of the DC-link capacitor. When Eq. (4) is used for the hot-spot temperature monitoring, high accuracy is hard to be reached since it only considers the fundamental-frequency ripples of the capacitor current. In fact, the high-frequency ripple currents absorbed by the DC-link capacitor will also contribute to certain amount of power losses, and thus contributing to temperature rise inside the DC-link capacitor of the PV system. Therefore, an accurate hot-spot monitoring and thus

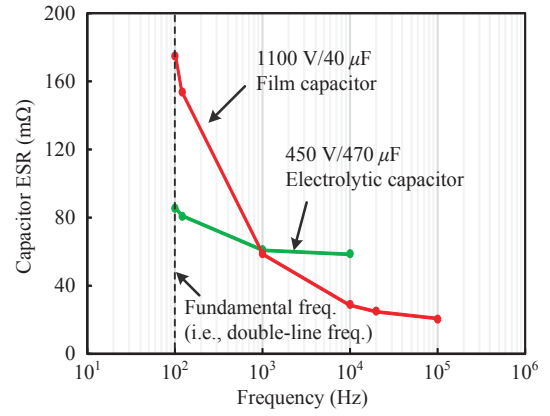


Fig. 4. Frequency dependency of the DC-link capacitor equivalent series resistor (ESR), where  $T_a = 25$  °C for test.

a reliability assessment of the DC-link capacitor requires a more detailed thermal model, where the effect from the high-frequency ripple currents flowing into the DC-link capacitor should also be taken into consideration and it will be discussed in details in the following.

### III. INSTANTANEOUS THERMAL MODELING

#### A. Frequency Dependency of the Capacitor ESR

In § II, it has been discussed that the high-frequency ripple current is also one of the contributors to the capacitor total power losses. However, simply replacing the fundamental current with high-frequency ripples in Eq. (3) and then summing up the power losses may result in error in the temperature estimation. This is due to that the capacitor ESR is of significant frequency dependency, as it is demonstrated in the experimental measurements in Fig. 4, where the ESRs of a film capacitor and an electrolytic capacitor were measured under different frequencies.

It can be observed in Fig. 4 that the ESR of either the film capacitor or the electrolytic capacitor has a significant change under different frequencies. Especially, the ESR of the film capacitor experienced a significant drop along with the frequency increase. In contrast, in a high frequency range (e.g., higher than 1000 Hz), the ESR of the electrolytic capacitor is almost constant, but an ESR difference can be still observed above the fundamental frequency. Therefore, in Fig. 4, it can be noted that the hot-spot temperature calculation of the DC-link capacitors according to Eq. (3) can lead to a relatively large error, and thus low confidence on the lifetime estimation. In the case of using a film capacitor as the DC-link capacitor, the frequency dependency of the capacitor ESR should be taken into consideration in order to achieve a reliable and accurate health monitoring of the DC-link capacitor.

#### B. Instantaneous Thermal Modelling of DC-Link Capacitors

Fig. 5 further shows a simulated example of the ripple current spectrum of the DC-link capacitor referring to Fig. 2. It has been demonstrated in Fig. 5 that the high-frequency ripple currents may also introduce significant power losses.

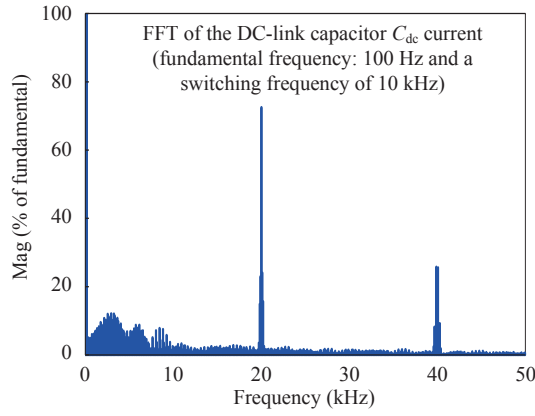


Fig. 5. An example of the harmonic spectrum (FFT - Fast Fourier Transform analysis) of the DC-link capacitor ripple current  $i_c$  of the PV system shown in Fig. 2, which is operating at its rated power (1000 W/m<sup>2</sup>, 25 °C).

Specifically, although the major harmonic component of the ripple current of the DC-link capacitor has a double-line frequency (i.e., 100 Hz), the high-order harmonic components of the switching frequency are not negligible. Therefore, when calculating the hot-spot temperature of the DC-link capacitor instantaneously, the power losses shown in Eq. (3) can be expressed in details as,

$$P_{c,loss} = \sum_{h=1}^N I_{ch}^2 R_{ESR}(f_h) \quad (5)$$

in which  $N$  is the number of the time-series points of the capacitor ripple current  $i_c$ ,  $I_{ch}$  is the RMS value of the capacitor harmonic currents, and  $R_{ESR}(f_h)$  is the corresponding ESR at the harmonic frequency  $f_h$  representing its frequency-dependency. Notably, the  $R_{ESR}(f_h)$  is usually provided in the data-sheet of the DC-link capacitor by the manufacturers. Otherwise, experimental measurements similar to those in Fig. 4 can be conducted in order to obtain the ESR at the corresponding frequency.

Actually, the measurements also enable a possibility to develop an instantaneous (frequency-dependent) ESR model by using curve-fitting. For example, the ESR of the capacitors shown in Fig. 4 exhibits an exponential decaying trend. Thus, an exponential ESR model can possibly be obtained within a certain frequency range as,

$$R_{ESR}(f_h) = R_{ESR}(100 \text{ Hz}) \left\{ 1 - A \cdot e^{-\frac{\beta}{f_h - 100}} \right\} \quad (6)$$

in which  $100 \leq f_h \leq f_m$  with  $f_m$  being the maximum frequency in the measurements,  $R_{ESR}(100 \text{ Hz})$  is the ESR at the fundamental frequency (i.e., 100 Hz),  $A$  and  $\beta$  are the fitting parameters that can be obtained in the curve-fitting process.

Consequently, an online Fast Fourier Transform (FFT) algorithm to the capacitor current can enable the instantaneous hot-spot temperature monitoring of the DC-link capacitor according to Eq. (5) and Eq. (6). The implementation of such a method to monitor the hot-spot temperature of DC-link

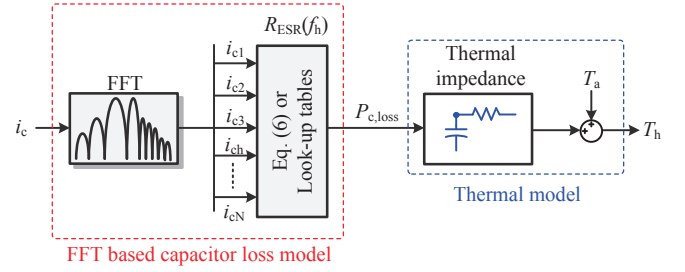


Fig. 6. Online fast Fourier transform (FFT) based instantaneous thermal modelling of the DC-link capacitor.

capacitors is shown in Fig. 6, where it is also observed that the look-up tables can be adopted for the  $R_{ESR}(f_h)$ . However, the FFT will consume massive computational resources and may introduce delays in a digital signal processor, which could result in an inaccuracy of the obtained hot-spot temperature of the DC-link capacitor.

In addition, inspired by the transient modelling approach introduced in [21], the instantaneous thermal loading of the DC-link capacitor can also be acquired by means of ripple current reconstruction, as it is illustrated in Fig. 7. It is known that the ripple current of the DC-link capacitor contains a double-frequency component ( $I_{c1}$ , 100 Hz) in the single-phase grid-connected systems (50 Hz grids), which can be calculated according to Eq. (2). Similarly, the high frequency harmonics  $I_{ch}$  can also be calculated based on the system operating conditions (e.g., the switching frequency  $f_{sw}$ , the duty cycle  $d$ , and etc). As a consequence, the total power losses of the DC-link capacitor can be obtained by using the look-up table or Eq. (6), leading to a real instantaneous hot-spot temperature monitoring of the DC-link capacitor.

Alternatively, an other simple way to monitor the hot-spot temperature is enabled by a direct look-table based loss model, as it is shown in Fig. 8, where the capacitor losses are directly linked with the solar irradiance level  $S$ , the ambient temperature  $T_a$ , and etc. Assuming that the harmonic distribution of the ripple current is equal under different environmental conditions, the look-up table based capacitor loss model can then be built up. As a result, it yet requires many off-line repeating simulations in order to obtain the ripple current distributions. Similar modelling has been introduced for the semiconductors in the PV inverters, as it has been presented in [2] and [20].

Fig. 7 actually provides a way to reconstruct the ripple current of the DC-link capacitor based on the system parameters/conditions. It can be implemented in the control system with additional sensors, which become the main drawback of this instantaneous monitoring method. Moreover, detailed mathematical derivations of this method (especially to calculate the ripple current components) have been another obstacle. Nevertheless, if the above issues can be solved, the ripple current reconstruction based instantaneous modelling method offers a possibility to derive the frequency domain models, e.g., from the input power to the hot-spot temperature.



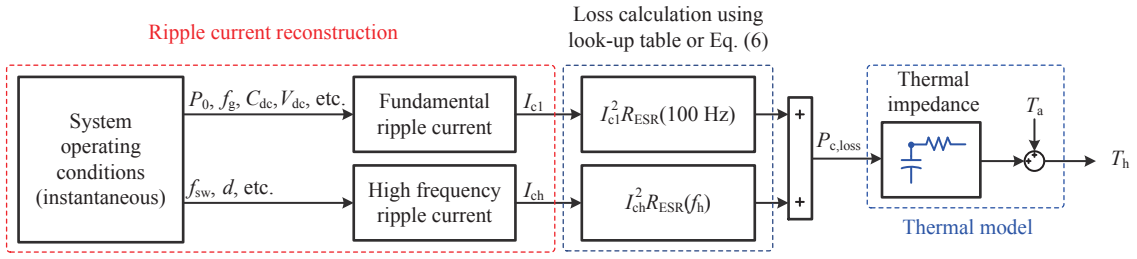


Fig. 7. Instantaneous thermal modelling for the DC-link capacitors based on the ripple current reconstruction method.

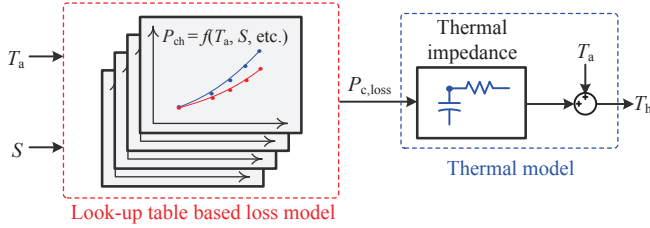


Fig. 8. Direct look-up table based instantaneous thermal modelling of the DC-link capacitor.

Consequently, the dynamics of the hot-spot temperature of the DC-link capacitor in response to the system conditions (e.g., solar irradiance changes, and other transients) can be assessed, which will be an extensive study of this paper.

### C. Modelling Method Comparison

All the above modelling approaches can enable an instantaneous monitoring of the DC-link capacitors in grid-connected PV systems. In terms of complexity, the look-up table based solution is the simplest one, but requiring many efforts to build up the look-up table. The accuracy of this instantaneous modelling approach thus is dependent of the "off-line" simulations that are performed. In contrast, the FFT based modelling method and the ripple current reconstruction solution are able to monitor the DC-link hot-spot temperature with high accuracy, and thus an accurate lifetime prediction of the DC-link capacitors can be achieved. However, the complexity is also increased in those approaches, especially for the ripple current construction based model. Considering the trade-off between the implementation complexity and the accuracy of the monitored hot-spot temperature, the look-up table based instantaneous modelling method is implemented in the following.

## IV. SIMULATION RESULTS

### A. Look-Up Table Implementation

Simulations have been performed on a 3-kW single-phase double-stage PV system like shown in Fig. 2, where the direct look-up table based instantaneous modelling approach shown in Fig. 8 has been adopted. The PV generator consists of 45 PV panels (i.e., three strings, 15 panels in each string), and the equivalent maximum power is 3 kW at 1000 W/m<sup>2</sup>, 25 °C with the voltage at the Maximum Power Point (MPP) being

TABLE II  
SPECIFICATIONS OF THE SELECTED DC-LINK CAPACITOR.

Parameter	Value
Rated capacitance	2200 $\mu$ F
Rated voltage	385 V
Maximum ESR at 20 °C, 100 Hz	38 m $\Omega$
Thermal resistance	2.3 °C/W

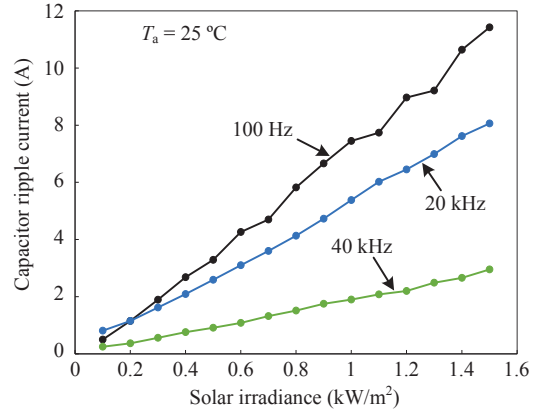


Fig. 9. Capacitor ripple currents (at 100 Hz, 20 kHz, and 40 kHz) under different solar irradiance levels, where  $T_a = 25$  °C.

266 V. A Perturb and Observe (P&O) MPPT algorithm [22] has been adopted to control the PV voltage. In the case that the DC-link voltage is controlled as:  $v_{dc}^* = 400 \pm 10$  V, two capacitors are connected in series as the DC-link, and Table II shows the specifications of the selected capacitor.

Firstly, the single-phase PV system is simulated under different ambient conditions, resulting in the possibility to extract the ripple current at different frequencies using the off-line FFT analysis. Fig. 9 shows the harmonics of the DC-link capacitor current at the fundamental frequency, 20 kHz and 40 kHz. It can be observed that, the high frequency ripple currents will also contribute to the total power losses of the DC-link capacitor. According to Eq. (5), the total power losses on the DC-link capacitor at constant solar irradiance and ambient temperature can be obtained as long as the corresponding ESR values ( $R_{ESR}(f_h)$ ) are known at those frequencies. In most cases,  $R_{ESR}(f_h)$  can be found in the data-sheet of the DC-link capacitor, as shown in Fig. 10; otherwise,

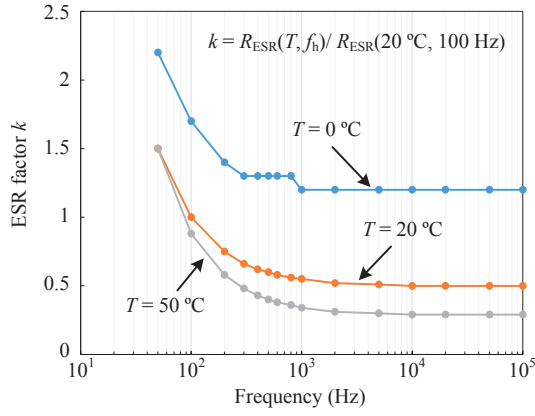


Fig. 10. Equivalent series resistance (ESR) frequency-dependency under different testing temperatures.

experimental measurements like the case shown in Fig. 4 should be conducted. Subsequently, by repeating off-line FFT analysis at different solar irradiance and ambient temperature conditions, a look-table can be built up, which takes the solar irradiance and ambient temperature as inputs and the output is the total power losses on the DC-link capacitor.

#### B. Examples under Daily Mission Profile of the PV Inverter

An application of the look-up table based instantaneous modelling has been performed on the single-phase grid-connected PV system. In that case, two daily operating conditions, as shown in Fig. 11, have been adopted as the inputs of the PV system. Then, the instantaneous thermal loading of the DC-link capacitor is translated from the two daily ambient conditions using the look-up table based instantaneous model of the DC-link capacitor, which are shown in Fig. 12.

As it can be seen in Fig. 12 that the look-up table based instantaneous modelling approach enables an effective translation of operating condition (mission profile) instantaneously to the thermal loading of the DC-link capacitor. Consequently, it is possible to monitor the hot-spot temperature of the DC-link capacitor during operation of the PV inverter, and also an online estimation of the capacitor operating hours can be achieved. Notably, in Fig. 12, only the power losses at the fundamental-frequency, the 20 kHz, and the 40 kHz are considered. Therefore, many transient characteristics of the DC-link capacitor cannot be observed from Fig. 12, but it can be enabled by the ripple reconstruction based instantaneous thermal modelling approach. Otherwise, in order to monitor the thermal dynamics of the DC-link capacitor, more ripple current components have to be taken into account.

In addition, compared to the thermal loading of the DC-link capacitor in [18], the estimated hot-spot temperature shown in Fig. 12(a) is lower. This is because in this paper the look-up table based model only considers the ripple currents of the DC-link capacitor at the fundamental-frequency, the 20 kHz, and the 40 kHz. In the case that more ripple current components are taken into consideration, a more accurate hot-spot temperature of the DC-link capacitor can be obtained.

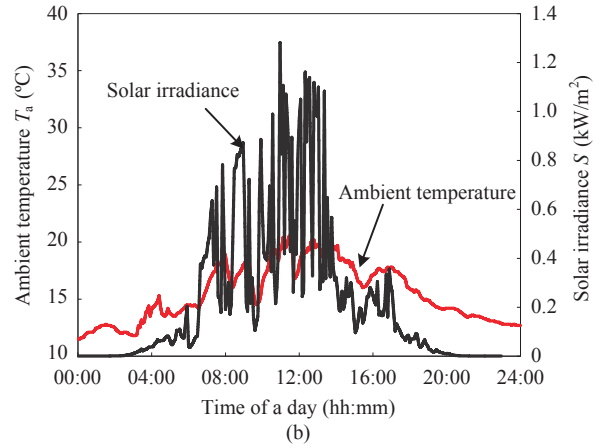
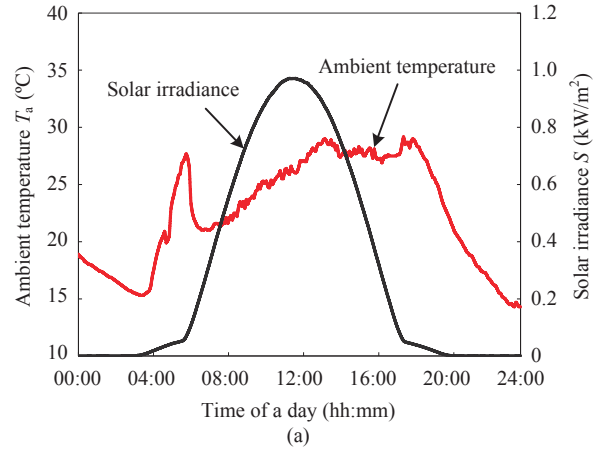


Fig. 11. Two daily operating conditions for the single-phase grid-connected PV system: (a) a clear day and (b) a cloudy day.

Nevertheless, the look-up table based instantaneous modelling reveals that high frequency ripple currents should also be considered in the thermal modelling of DC-link capacitor in order to achieve a more accurate temperature monitoring and thus a lifetime estimation of the DC-link capacitor.

## V. CONCLUSION

In this paper, instantaneous thermal modelling approaches of the DC-link capacitor in grid-connected PV systems have been explored. The presented instantaneous thermal modelling solutions are based on Fast Fourier Transform (FFT), look-up tables, and ripple current reconstruction. In contrast to the FFT based hot-spot temperature monitoring approach, the look-up table based method is easier to be implemented, but it can still enable an instantaneous translation to the thermal loading of the DC-link capacitors from long-term operating conditions. In terms of high accuracy, the ripple current reconstruction based instantaneous modelling approach offers a possibility to analyze the dynamic thermal performance of the DC-link capacitors in the frequency domain. Since the transients are more challenging to the DC-link capacitor lifetime, the instantaneous modelling approaches are of meaningfulness to

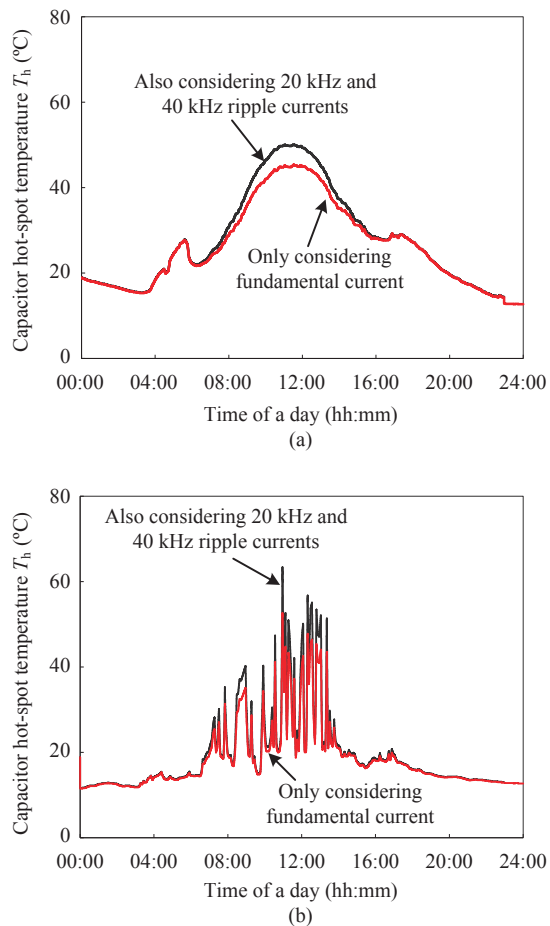


Fig. 12. Hot-spot temperature of the DC-link capacitor in the 3-kW single-phase grid-connected PV system shown in Fig. 2 with the look-up table based instantaneous thermal monitoring approach under two daily operating conditions: (a) a clear day and (b) a cloudy day.

the future DC-link capacitor design. It is necessary to include high-frequency components for the loss/thermal estimation to the DC-link capacitors. Taking two real-field daily ambient operations as example, simulations on a 3-kW single-phase grid-connected PV systems have been adopted to demonstrate the look-up table based instantaneous thermal modelling approach for the DC-link capacitor.

## REFERENCES

- [1] S. Yang, A. Bryant, P. Mawby, D. Xiang, L. Ran, and P. Tavner, "An industry-based survey of reliability in power electronic converters," *IEEE Trans. Ind. Appl.*, vol. 47, no. 3, pp. 1441–1451, May 2011.
- [2] K. Ma, Y. Yang, H. Wang, and F. Blaabjerg, "Design for reliability of power electronics in renewable energy systems," in *Use, Operation and Maintenance of Renewable Energy Systems*. Springer, 2014, pp. 295–338.
- [3] H. Wang and F. Blaabjerg, "Reliability of capacitors for DC-link applications in power electronic converters - an overview," *IEEE Trans. Ind. Appl.*, vol. 50, no. 5, pp. 3569–3578, Sept. 2014.
- [4] T. Messo, J. Jokipii, J. Puukko, and T. Suntio, "Determining the value of DC-link capacitance to ensure stable operation of a three-phase photovoltaic inverter," *IEEE Trans. Power Electron.*, vol. 29, no. 2, pp. 665–673, Feb. 2014.
- [5] J.D. van Wyk and F.C. Lee, "On a future for power electronics," *IEEE J. Emerging and Selected Topics in Power Electron.*, vol. 1, no. 2, pp. 59–72, Jun. 2013.
- [6] F. Blaabjerg and K. Ma, "Future on power electronics for wind turbine systems," *IEEE J. Emerging and Selected Topics in Power Electron.*, vol. 1, no. 3, pp. 139–152, Sept. 2013.
- [7] B. Ji, X. Song, E. Sciberras, W. Cao, Y. Hu, and V. Pickert, "Multi-objective design of IGBT power modules considering power cycling and thermal cycling," vol. PP, no. 99, pp. 1–12, in press, 2015.
- [8] H. Wang, M. Liserre, F. Blaabjerg, P. de Place Rimmen, J.B. Jacobsen, T. Kvisgaard, and J. Landkildehus, "Transitioning to physics-of-failure as a reliability driver in power electronics," *IEEE J. Emerging and Selected Topics in Power Electron.*, vol. 2, no. 1, pp. 97–114, Mar. 2014.
- [9] V. Andoralov, C. Larsson, and L. Eliasson, "Progress in performance of high voltage aluminum electrolytic capacitors," in *Proc. of PCIM Europe*. VDE, pp. 1-5, 20-22 May 2014.
- [10] S.B. Kjaer, J.K. Pedersen, and F. Blaabjerg, "A review of single-phase grid-connected inverters for photovoltaic modules," *IEEE Trans. Ind. Appl.*, vol. 41, no. 5, pp. 1292–1306, Sept. 2005.
- [11] K. Lee, T.M. Jahns, T.A. Lipo, G. Venkataramanan, and W.E. Berkopec, "Impact of input voltage sag and unbalance on DC-link inductor and capacitor stress in adjustable-speed drives," *IEEE Trans. Ind. Appl.*, vol. 44, no. 6, pp. 1825–1833, Nov. 2008.
- [12] E.C. Aeloiza, J.-H. Kim, P.N. Enjeti, and P. Ruminot, "A real time method to estimate electrolytic capacitor condition in PWM adjustable speed drives and uninterruptible power supplies," in *Proc. of PESC*, pp. 2867–2872, Jun. 2005.
- [13] A. Wechsler, B.C. Mecrow, D.J. Atkinson, J.W. Bennett, and M. Benarous, "Condition monitoring of DC-link capacitors in aerospace drives," *IEEE Trans. Ind. Appl.*, vol. 48, no. 6, pp. 1866–1874, Nov. 2012.
- [14] M.A. Vogelsberger, T. Wiesinger, and H. Ertl, "Life-cycle monitoring and voltage-managing unit for DC-link electrolytic capacitors in PWM converters," *IEEE Trans. Power Electron.*, vol. 26, no. 2, pp. 493–503, Feb. 2011.
- [15] H. Hu, S. Harb, N. Kutkut, I. Batarseh, and Z.J. Shen, "A review of power decoupling techniques for microinverters with three different decoupling capacitor locations in PV systems," *IEEE Trans. Power Electron.*, vol. 28, no. 6, pp. 2711–2726, June 2013.
- [16] M.A. Brubaker, D. El Hage, T.A. Hosking, H.C. Kirbie, and E.D. Sawyer, "Increasing the life of electrolytic capacitor banks using integrated high performance film capacitors," in *Proc. of PCIM Europe*, pp. 206–213, 14-16 May 2013.
- [17] M.L. Gasperi, "Life prediction modeling of bus capacitors in AC variable-frequency drives," *IEEE Trans. Ind. Appl.*, vol. 41, no. 6, pp. 1430–1435, Nov. 2005.
- [18] Y. Yang, K. Ma, H. Wang, and F. Blaabjerg, "Mission profile translation to capacitor stresses in grid-connected photovoltaic systems," in *Proc. of ECCE*, pp. 5479–5486, Sept. 2014.
- [19] J.N. Davidson, D.A. Stone, and M.P. Foster, "Required cauer network order for modelling of thermal transfer impedance," *IET Electronics Letters*, vol. 50, no. 4, pp. 260–262, Feb. 2014.
- [20] H. Huang and P.A. Mawby, "A lifetime estimation technique for voltage source inverters," *IEEE Trans. Power Electron.*, vol. 28, no. 8, pp. 4113–4119, Aug. 2013.
- [21] K. Ma, Y. Yang, and F. Blaabjerg, "Transient modelling of loss and thermal dynamics in power semiconductor devices," in *Proc. of ECCE*, pp. 5495–5501, Sept. 2014.
- [22] N. Femia, G. Petrone, G. Spagnuolo, and M. Vitelli, "Optimization of perturb and observe maximum power point tracking method," *IEEE Trans. Power Electron.*, vol. 20, no. 4, pp. 963–973, Jul. 2005.